Floquet Prethermalization with Lifetime Exceeding 90 s in a Bulk Hyperpolarized Solid

William Beatrez, Otto Janes, Amala Akkiraju, Arjun Pillai, Alexander Oddo, Paul Reshetikhin, Emanuel Druga, Maxwell McAllister, Mark Elo, Benjamin Gilbert, Dieter Suter, and Ashok Ajoy

Floquet prethermalization with lifetime exceeding 90s in a bulk hyperpolarized solid

William Beatrez,[1] Otto Janes,[1] Amala Akkiraju,[1] Arjun Pillai,[1] Alexander Oddo,[1] Paul Reshetikhin,[1]
Emanuel Druga,[1] Maxwell McAllister,[1] Mark Elo,[2] Benjamin Gilbert,[3] Dieter Suter,[4] and Ashok Ajoy[1,5,*]

[1]*Department of Chemistry, University of California, Berkeley, Berkeley, CA 94720, USA.*
[2]*Tabor Electronics Inc. Hatasia 9, Nesher, 3660301, Israel.*
[3]*Energy Geoscience Division, Lawrence Berkeley National Laboratory, Berkeley, CA 94720, USA.*
[4]*FakultÃdĭ Physik, Technische UniversitÃdĭ Dortmund, D-44221 Dortmund, Germany.*
[5]*Chemical Science Division, Lawrence Berkeley National Laboratory, University of California, Berkeley, Berkeley, CA 94720, USA.*

We report the observation of long-lived Floquet prethermal states in a bulk solid composed of dipolar-coupled ^{13}C nuclei in diamond at room temperature. For precessing nuclear spins prepared in an initial transverse state, we demonstrate pulsed spin-lock Floquet control that prevents their decay over multiple-minute long periods. We observe Floquet prethermal lifetimes $T_2' \approx 90.9$s, extended >60,000-fold over the nuclear free induction decay times. The spins themselves are continuously interrogated for ~10min, corresponding to the application of ≈5.8M control pulses. The ^{13}C nuclei are optically hyperpolarized by lattice Nitrogen Vacancy (NV) centers; the combination of hyperpolarization and continuous spin readout yields significant signal-to-noise in the measurements. This allows probing the Floquet thermalization dynamics with unprecedented clarity. We identify four characteristic regimes of the thermalization process, discerning short-time transient processes leading to the prethermal plateau, and long-time system heating towards infinite temperature. This work points to new opportunities possible via Floquet control in networks of dilute, randomly distributed, low-sensitivity nuclei. In particular, the combination of minutes-long prethermal lifetimes and continuous spin interrogation opens avenues for quantum sensors constructed from hyperpolarized Floquet prethermal nuclei.

Introduction – Systems pulled away from thermal equilibrium can exhibit unusual phenomena non-existent or difficult to achieve at equilibrium [1]. For instance, periodically driven quantum systems can display long-lived prethermal lifetimes due to the emergence of approximately conserved quantities under the effective time-independent Hamiltonian describing the drive [2–6]. For sufficiently large driving frequencies ω, much higher than the intrinsic energy scales in the system Hamiltonian (hereafter J), these prethermal lifetimes scale exponentially with ω [7–11]. Ultimately, however, the system absorbs energy and âĂIJheats upâĂİ to a featureless infinite temperature state.

The long-lived prethermal plateau and its stability against perturbations in the drive portends applications for the engineering of quantum states [3, 4, 12]. Fundamentally, the control afforded by periodically driven systems opens avenues to study non-equilibrium phenomena and explore novel dynamic phases of matter, some of which have no equilibrium counterparts [13, 14]. A flurry of theoretical work has recognized Floquet prethermalization under random driving [15], in driven linear chains [10], and even in the classical limit [16]. Experimentally, Floquet prethermalization has been observed recently in cold-atom [17–19] and NMR systems [20–22]. They demonstrated a characteristic exponential suppression of heating rates with Floquet driving. Even before the current resurgence of interest, decades-old NMR experiments had observed certain signatures of prethermalization, then referred to as âĂIJquasi-equilibriumâĂİ [23–28].

In this Letter, we report observation of Floquet prethermal states with lifetimes exceeding 90s at room temperature in a dipolar-coupled ensemble of ^{13}C nuclei in diamond (see Fig. 1A). These nuclear spins, *randomly* positioned at 1% concentration in the lattice, are optically hyperpolarized by interactions with NV defect centers, which enhances their polarization ε=223-fold with respect to the thermal limit (Fig. 1B). When
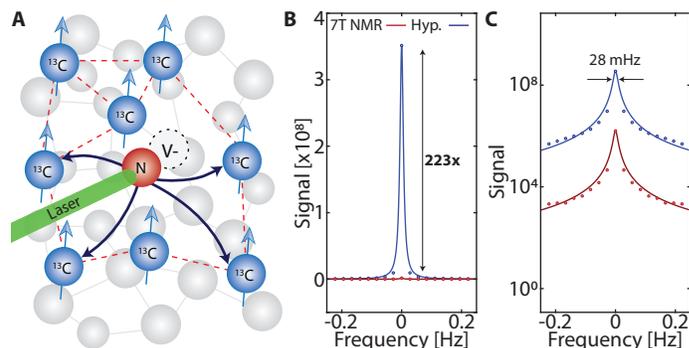
Fig. 1. **System.** (A) Dipolar lattice of ^{13}C nuclei in diamond. Optically pumped NV centers are employed to hyperpolarize the ^{13}C nuclei (blue arrows). (B-C) *Signal gains from hyperpolarization*, demonstrated by comparing *single-shot* ^{13}C NMR spectra to conventional 7T (thermal) NMR. Data is shown in (B) linear and (C) log scales; line is a fit. Here, optical pumping was for 2min at 36mT, and thermal measurement was taken after 4hrs in the magnet.

placed in a Bloch transverse state $\hat{\mathbf{x}}$ in the absence of periodic driving, these precessing nuclei naturally dephase with free induction decay lifetime $T_2^* \approx 1.5$ms and measured observables decay to zero. Under rapid pulsed spin-lock driving, however, we are able to effect a significant improvement; the observed lifetimes $T_2 \approx 90.9$s constitute a >60,000-fold extension over T_2^*. Moreover, with a drive consisting of ≈5.8M pulses, we are able to continuously probe the thermalization process for up to 573s with high fidelity. This corresponds to >10^{10} precession cycles of the nuclear spins. Both with respect to the number of pulses applied, and the ultimate transverse spin lifetimes, these values are amongst the largest reported in literature [29, 30]. Our work therefore suggests interesting opportunities for Floquet control afforded in hyperpolarizable spin networks consisting of dilute low-gyromagnetic ratio nuclei [31].

A primary contribution in this work is the ability to probe the system thermalization dynamics with unprecedented signal-
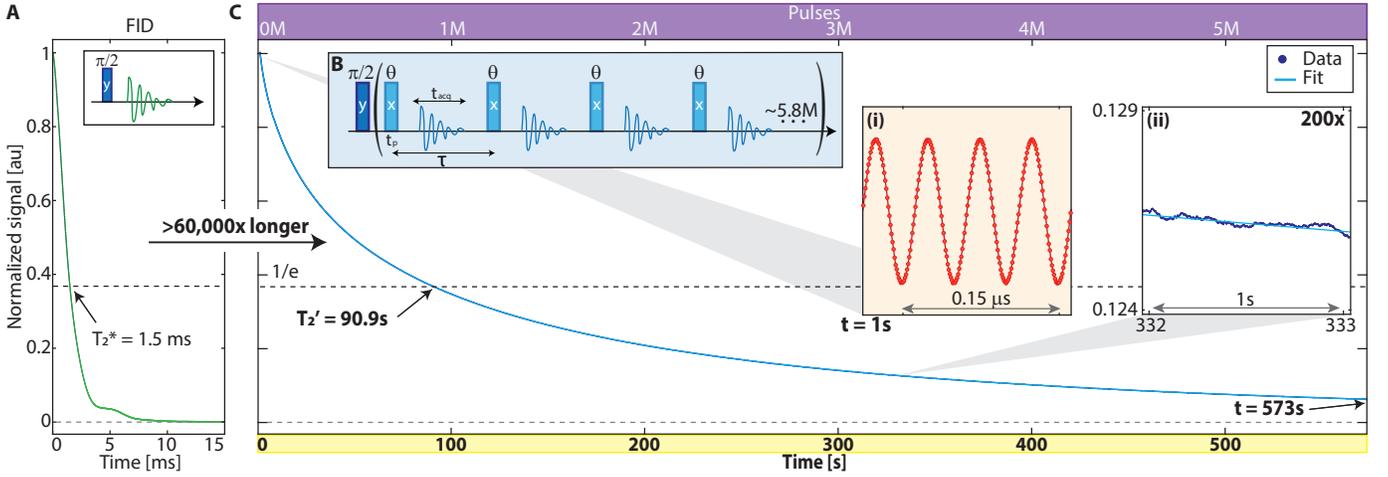
Fig. 2. **Floquet driving and lifetime extension.** (A) Conventional ^{13}C free induction decay with $T_2^* \approx 1.5$ms. (B) *Floquet drive* consists of a train of ϑ-pulses applied spin-locked with the ^{13}C nuclei. Spins are interrogated in t_{acq} windows between the pulses (blue lines), the nuclear precession is sampled every 1ns. Pulse repetition rate $\omega = \tau^{-1}$, and sequence not drawn to scale. (C) *Minutes-long lifetimes* of the transverse state result from the Floquet sequence ($\vartheta \approx \pi/2$). Data (blue points) shows *single-shot* measurement of survival probability in the state ρ_I, and line is a fit to a sum of five exponentials. Here $t_{acq}=2\mu$s, $t_p=40\mu$s and $\tau=99.28\mu$s, and the 573s period corresponds to ≈ 5.8M pulses (upper axis). We neglect here the first 100ms for clarity (see Fig. 3A). *Inset (i)*: Raw data showing measurement of the ^{13}C spin precession, here at 1s into the decay. *Inset (ii)*: Data zoomed 200x in a 1s window. Using a $1/e$-proxy yields $T_2 \approx 90.9$s. This corresponds to a $>60,000$-fold extension compared to the FID.

to-noise (SNR). Integrated SNR (see Fig. 1B-C) exceeds 10^8 per shot, including $>10^3$ per data point (for nearly all ≈ 5.8M points), arising from a combination of hyperpolarization and continuous spin readout in our experiments. When $\vartheta \approx \pi/2$, this amounts to >1.4M Floquet cycles. This permits a view into the thermalization process with a high degree of clarity, in a manner not directly accessible in previous experiments. Not only does our experiment allow high-SNR continuous-readout access to very large numbers of Floquet cycles, but also offers the ability to discern dynamics within individual cycles. This is an important distinction from simple Magnus expansion treatments, which only give information on stroboscopic dynamics.

We are able to identify the four smoothly transitioning thermalization regimes that confirm theoretical predictions [32] âĂŤ an initial transient to the prethermal plateau, the crossover to unconstrained thermalization and, ultimately, infinite temperature. High measurement SNR also allows characterization of heating rates over a wide range of drive frequencies. We observe system heating scaling $\propto \exp(-t^{1/2})$ at high drive frequency ω. Simultaneously, the transient system response unveils interesting harmonic behavior while establishing the prethermal plateau.

System – In a magnetic field $\mathbf{B}_0$, the ^{13}C nuclei interact by the dipolar Hamiltonian, $\mathcal{H}_{dd} = \sum_{j<k} d_{jk}^{CC}(3I_{jz}I_{kz} - \vec{I}_j \cdot \vec{I}_k)$, with a coupling strength $d_{jk}^{CC} = \frac{\mu_0}{4\pi}\hbar\gamma_n^2(3\cos^2\beta_{jk}-1)\frac{1}{r_{jk}^3}$, where I refer to spin-1/2 Pauli matrices, $\gamma_n=10.7$MHz/T is the gyromagnetic ratio, and $\beta_{jk} = \cos^{-1}\left(\frac{\mathbf{r}_{jk}\cdot\mathbf{B}_0}{r_{jk}B_0}\right)$ is the angle of the internuclear vector $\mathbf{r}_{jk}$ to the magnetic field. The sample is oriented with $\mathbf{B}_0||[100]$, such that nearest neighbor (NN) ^{13}C sites are decoupled. Ultimately, the median dipolar coupling is $J = \langle d_{jk}^{CC} \rangle \approx 0.66$kHz (Fig. 2A). The random ^{13}C distribution leads to a long tailed distribution in the coupling values, effectively rendering the interaction Hamiltonian *disordered*.

In addition, the nuclei are subject to on-site disorder, i.e. local dephasing fields, $\mathcal{H}_z = \sum_j c_j I_{jz}$, arising from interactions with paramagnetic impurities (e.g. P1 centers) [33]. At typical 20ppm P1 concentrations, $\langle c_j^2 \rangle \approx 0.4[\text{kHz}]^2$ [34]. In the rotating frame of the Floquet drive, the ^{13}C Hamiltonian is therefore $\mathcal{H} = \mathcal{H}_{dd} + \mathcal{H}_z$.

Compared to previous NMR experiments, our work introduces some special features leveraging nuclear hyperpolarization [25, 26]. The vast preponderance of NMR experiments have been limited to high-γ_n and dense (100% abundant) nuclei such as ^{19}F, ^{31}P, and ^{1}H [20, 22]. Instead, we focus attention to dilute networks of insensitive nuclei (^{13}C). This provides a combination of factors critical to establishing Floquet control for long periods âĂŤ *(i)* a relatively low $\|\mathcal{H}_{dd}\|$ compared to networks constructed from sensitive (high-γ_n) nuclei, scaling as $\eta^{1/2}\gamma_n^2$, where η is the nuclear enrichment, *(ii)* a long tailed distribution in couplings, and *(iii)* long nuclear T_1 (here ≈ 25 min), significantly higher than many experimental systems, sets a long memory time for the nuclear states.

Indeed, these very factors, while attractive for Floquet control [30], usually make experiments challenging on account of poor sensitivity. Inductively measured nuclear signals scale $\propto \gamma_n^2$, with a measurement repetition rate set by T_1^{-1}, making obtaining reasonable SNR a challenge [35]. We mitigate these difficulties by a combination of hyperpolarization and instrumental advances (allowing continuous sampling). Hyperpolarization is carried out at $B_{pol}=36$mT through a method previously described [36, 37]. Measurement throughput is accelerated by $\approx \frac{1}{2}\varepsilon^2\left[T_1(B_0)/T_1(B_{pol})\right]^2\frac{T_2}{T_2^*} \gtrsim 10^{10}$ over conventional high-field (FID-based) NMR readout.

Floquet control and measurement âĂŤ The driving protocol is described in Fig. 2B [40–42]. Post polarization, the ^{13}C nuclei are rotated to transverse axis $\hat{\mathbf{x}}$ on the Bloch sphere, placing them in an initial state $\rho_I \sim \varepsilon I_x$. The Floquet drive consists of
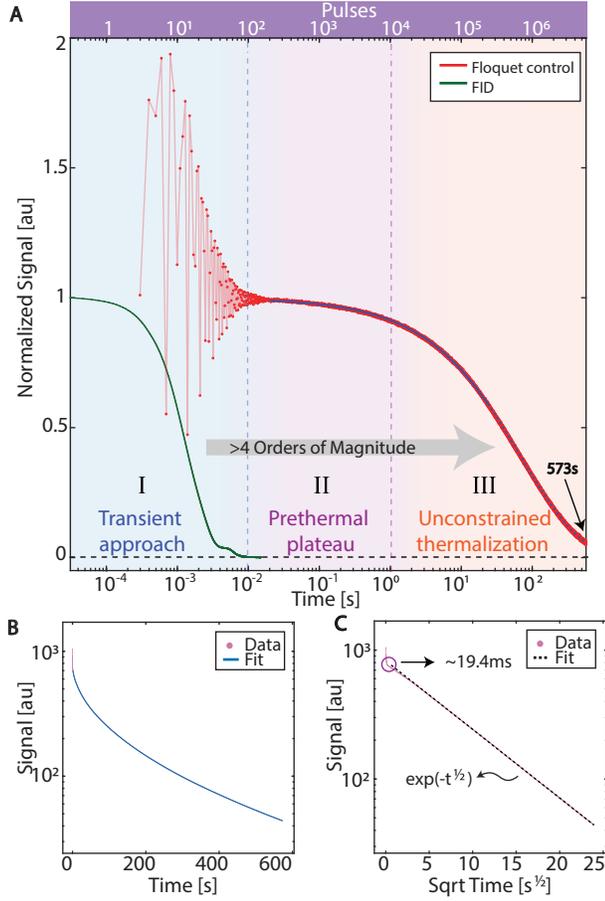
Fig. 3. **Floquet thermalization regimes** (A) *Log-scale* visualization of the full data in Fig. 2C. Points are experiment, there are ≈5.8M data points here. Upper axis denotes number of pulses applied, here $J\tau \approx 0.066$. Green points are the FID. We observe distinct, yet smoothly transitioning (shaded), thermalization regimes (**I-IV**): a ≈10ms oscillatory approach (**I**) to the Floquet prethermal plateau (**II**), followed by unconstrained thermalization (**III**). Infinite temperature regime (**IV**) is not reached in these measurements up to 573s. (B) *Semi-log* plot of the experimental data shows a dynamic change of thermalization rate. (C) *Semi-log plot against* $\sqrt{t}$ yields an approximately linear dependence (dashed line) for ~500s. Cusp (marked) at ≈9.2ms marks transition to the prethermal plateau (regime **II**, see also Fig. 5).

Fig. 4. **Exponential dependence of Floquet prethermal lifetimes.** (A) *Variation with $J\tau$*. Data (points) shows measured signal probing thermalization dynamics in regime **II-III** for representative $J\tau$ values (colorbar). Here $\vartheta \approx \pi/2$ and $t_{\text{acq}}=32\mu s$ and there are a high number (~10^3-10^6) points per line [38]. Data is normalized at the transition points to the prethermal plateau (following Fig. 3C). The Floquet prethermal decay rates reduce considerably with decreasing $J\tau$. See full data at Ref. [39]. *Inset:* Zoom-in (on semilog scale). (B) *Extracted decay rates* focusing on the region where decay follows ~$\exp(-t^{1/2})$. Plotted in a semi-log scale against ω/J, the dashed line reveals an approximately exponential scaling of the decay rates at low drive frequencies ω (dashed line is a linear fit). At high ω we observe sharp narrow features in the prethermal decay rates. (C) *Plotted against $J\tau$*, showing exponential scaling at higher drive frequency (dashed line). Narrow features in the decay rates superimposed on the exponential background are more emphasized here. (D) *Log-scale plot* of the extracted T_2 lifetimes against ω. Dashed line is a linear fit.

an equally spaced train of pulses of flip angle ϑ. The center-to-center pulse separation is $\tau\left[=(\omega/2\pi)^{-1}\right]$. After N pulses, the unitary operator describing its action in the rotating frame can be written as, $U(N\tau) = \left[\exp(i\vartheta I_x)\exp(i\mathcal{H}\tau)\right]^N$, where we have made a simplifying assumption of δ-pulses. The data is sampled after every pulse, $t_j=j\tau$, and the evolution can be described by the operation $U(t) = \prod_{j=1}^{N} \exp(i\mathcal{H}^{(j)}\tau)$, where we refer to the toggling frame Hamiltonians after every pulse [43], $\mathcal{H}^{(j)} = \exp(ij\vartheta I_x)\mathcal{H}\exp(-ij\vartheta I_x)$. This evolution can be recast as, $U(t) = \exp(i\mathcal{H}_F N\tau)$, where H_F is the Floquet Hamiltonian that captures the system dynamics under the drive. $\mathcal{H}_F$ can be expanded in a Floquet-Magnus expansion [44–46] to leading order in the parameter $\zeta=2\pi J/\omega$, and in the regime $\zeta \ll 1$, yields

a time independent Hamiltonian,

$$\mathcal{H}_F^{(0)} = \sum_{j=1}^{N} \mathcal{H}^{(j)} \approx \sum_{j<k} d_{jk}^{\text{CC}}\left(\frac{3}{2}\mathcal{H}_{\text{ff}} - \vec{I}_j \cdot \vec{I}_k\right), \quad (1)$$

with the flip-flop Hamiltonian, $\mathcal{H}_{\text{ff}} = I_{jz}I_{kz}+I_{jy}I_{ky}$ [47]. The $\mathcal{H}_z$ dephasing fields are filtered out in $\mathcal{H}_F^{(0)}$. For sufficiently small ζ, Eq. (1) holds irrespective of the flip-angle ϑ, except for certain special values ($\vartheta \approx \pi, 2\pi$). We note that this constitutes a key difference with respect to conventional dynamical decoupling control (CPMG [48]), wherein the interspin couplings are retained and result in rapid ^{13}C decay [47]. The higher order terms in the Magnus expansion are progressively smaller, but contribute to long time system dynamics [45, 49]. Importantly, the initial transverse magnetized state ρ_I is a conserved quantity under $\mathcal{H}_F^{(0)}$, since $[\rho_I, \mathcal{H}_F^{(0)}]=0$. This leads to prethermal lifetimes that depend exponentially on the drive frequency ω. Ultimately, the divergence of the expansion manifests in the

system heating to infinite temperature.

Fig. 2C shows the measured survival probability $F(N\tau)$ of the state ρ_I under the applied Floquet drive. This can be expressed as, $F(N\tau) = \frac{1}{2}\text{Tr}\{\rho_I U(N\tau)^\dagger \rho_I U(N\tau)\}$. We have neglected the first 100ms here for clarity (see Fig. 3A for full data). Data shows significant extension in the transverse state lifetimes. Points in Fig. 2C are the experimental data while the line is a fit to a sum of five exponentials (zoomed in Fig. 2C(ii)); the high measurement SNR is evident in the zoomed data. The product $J\tau$ is a convenient metric to label the Floquet regime of operation, and in these measurements $J\tau=0.066$. The $\vartheta\approx\pi/2$ pulses here are applied every $\tau\approx100\mu$s, and the 573s period encapsulates ≈5.8M pulses. For comparison, the conventional ^{13}C free induction decay [50] in the absence of Floquet driving is shown in Fig. 2A, where decay occurs in $T_2^*\approx1.5$ms on account of internuclear couplings and static field disorder. High SNR and continuous weak measurement readout allows us to recognize (see Fig. 3B) a dynamic change in the decay rate constant along the curve, making it difficult to quantify the decay rate by a single number. The data especially past 100ms is found to fit well to the stretched exponential $\sim\exp\left[-(t/T_2)^{1/2}\right]$, from where we extract $T_2=66.7$s. Alternatively, using a $1/e$- intersection (dashed line in Fig. 2C) as a convenient proxy yields, $T_2=90.9$s. The extension leads to substantial line-narrowing of the ^{13}C NMR spectrum (~28mHz in Fig. 1C).

The measurement procedure for Fig. 2C is detailed in the Supplementary Information [38]. The signal is sampled every 1ns in t_{acq} windows between the pulses (see Fig. 2B). The maximum memory size, 16GB, limits detection to 12 billion 12-bit samples. Even for a $t_{\text{acq}}=2\mu$s window as in Fig. 2C, this currently limits total acquisition period to 10min. In any case, such continuous readout (akin to weak measurement [51]) yields significant SNR advantages over point-by-point stroboscopic measurements. Rapid data sampling throughput (at $f_s=\tau^{-1}$) also allows further filtering to be applied when the dynamics are slow compared to f_s. With this, we obtain a single-shot SNR $>10^3$ per measurement point, and $\approx5\times10^8$ for the integrated signal (see Fig. 1C).

Floquet Prethermalization – To better illustrate thermalization dynamics of the spins, Fig. 3A shows the full data on a logarithmic time scale. The FID is also shown, and lifetime extension is evident from the shift in the curves. Points are experimental data with no moving average applied, and the solid and dashed lines are stretched exponential fits. We identify distinct, albeit smoothly transitioning, regimes in the thermalization process (shaded in Fig. 3A). Following Ref. [2], we refer to them as: **(I)** an initial regime of constrained thermalization ($0<t<20$ms), where we observe oscillatory behavior with a harmonic frequency response of the Floquet drive frequency ω, **(II)** the prethermal plateau, leading into **(III)** unconstrained thermalization towards the **(IV)** infinite temperature state (not reached in these experiments).

Let us first focus our attention to the dynamics in regimes **II** and **III**. Fig. 3B-C shows two complementary visualizations after moving average filter is applied over the entire data. Fig. 3B, plotted on a semi-log scale, makes evident that the decay rate constant changes over the entire thermalization period. The high SNR and rapid sampling rate, however, allows us to unravel the exact rate change behavior in a manner not accessible in previous experiments. It is easiest seen when re-plotted against $\sqrt{t}$ in Fig. 3C, where we obtain an approximately linear trend (dashed
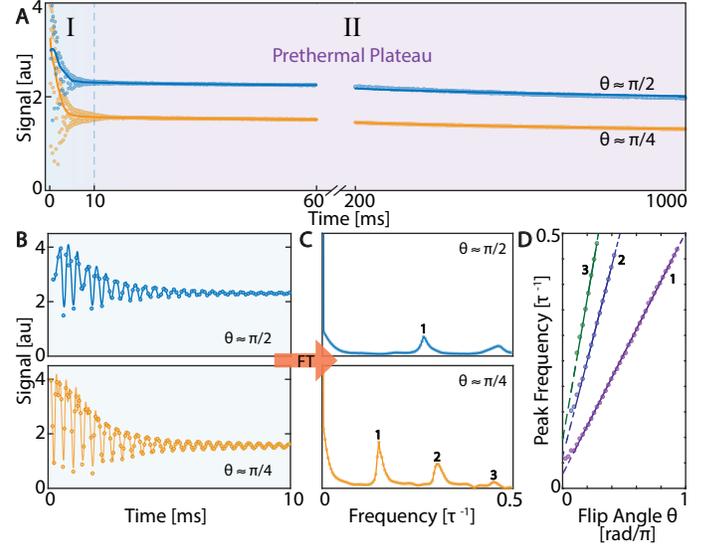
Fig. 5. **Transient approach to prethermal plateau.** (A) *Oscillations in the approach to prethermal plateau* seen for data zooming in on region **I**, in a 1s long window (see Fig. 3A). Data (points) corresponds to $\vartheta\approx\{\pi/2,\pi/4\}$ respectively. Solid line is data with moving average filtering applied over the entire region (see Fig. 3B). (B) *Zoom in* to region **I** shows the transient approach with high SNR. It is evident that the oscillations are at higher frequency for $\vartheta\approx\pi/2$. Solid line is a spline fit to guide the eye. (C) *Fourier transforms* of panels in B allows identification of the frequency components constituting the oscillations as a function of $\omega=\tau^{-1}$. Harmonics are represented by numbers. It is clear that primary oscillation frequency is higher for $\vartheta\approx\pi/2$, where we extract the primary harmonic position at $\approx0.26\tau^{-1}$. (D) *Variation with flip angle ϑ*. Data shows the position of the oscillation frequency for the primary and higher harmonics (numbered). See full data at Ref. [52]. Solid lines are linear fits, while dashed line is an extrapolation. Slopes are in the ratio expected.

line) over a long period (~500s). The prethermal dynamics is therefore $\sim\exp(-t^\alpha)$ with exponent $\alpha\approx1/2$. Decades-old NMR experiments had observed a similar trend in paramagnetic impurity rich solids [53, 54]. We emphasize however the high SNR of the data in Fig. 3, proffering insights into, and deviations from, this behavior. At higher $J\tau$ values, for instance, we observe a dynamic decrease in α away from 1/2 in regime **III** (movie available at Ref. [39]). The turning point (cusp) in data in Fig. 3C, obtained after moving average filtering over the oscillations in regime **I**, also allows a convenient means to quantify the exact point of transition to prethermal plateau. The length of this period (≈10-20ms) closely mirrors the period over which the FID completely decays (see Fig. 3A).

To study the scaling of the prethermal lifetimes with the frequency of the Floquet drive ω, Fig. 4A shows similar data at a range of $J\tau$ values. This is carried out by varying the inter-pulse spacing τ in Fig. 2B. The full dataset (shown in Supplementary Information) consists of measurements at 57 such $J\tau$ values, but we show a restricted set here for clarity. Again, there is a high density of data points in each experimental line. To restrict attention to regions **II-III**, we normalize the data at the transition points to the prethermal plateau, identified from the cusps as in Fig. 3C. The data show thermalization proceeding more slowly for lower values of $J\tau$. The dynamic change of rate coefficient makes plotting a single graph that encapsulates

the full long-time behavior difficult. Instead, we extract the decay rates focusing on regimes **II-III**, where decay (similar to Fig. 3C) follows an exponent $\alpha \approx 1/2$.

This is presented in two complementary viewpoints in Fig. 4B-C. First, in Fig. 4B plotted on a semi-log scale with respect to the drive period τ, we see a linear trend in the decay rates, especially at high τ (dashed line). This points to an approximately exponential scaling of the state preservation lifetimes with drive frequency, one of the signatures of Floquet prethermalization. At low τ however, we observe a flatter slope with sharp features in the decay rates. Fig. 4C shows an alternate view instead in terms of ω. Extracting the transverse state lifetimes T_2 on the log-log plot, we find a slope of 2.1 ± 0.1 at low-frequency suggesting a Fermi's Golden Rule scaling with drive frequency [55]. Since Rabi frequency is relatively low in our experiments, the lowest $J\tau$ value accessible was 0.066. We estimate that the filling factor of the RF coil employed for ^{13}C readout in our experiments can be improved by about an order of magnitude. The scaling observed in Fig. 4 suggests that such an improvement in $J\tau$ would result in significant gains in T_2 lifetimes.

The sharp peaks in the decay rates in the high ω regime in Fig. 4B-C are intriguing. We believe this is a manifestation of quantum sensing âĂŤ the ^{13}C nuclei see an enhanced decay rate when subjected to environmental magnetic fields at a fixed frequency f_{ac} matched in periodicity (resonant) with the pulse sequence, at $f_{ac}=\vartheta/(2\pi\tau)$. The first two peaks are observed at $f_{ac}\approx2.5$kHz and $f_{ac}\approx5.0$kHz. This is possible because the pulsed spin-lock sequence exhibits dynamical decoupling properties similar to quantum sensing protocols [31]. The exact origin of these fields in Fig. 4B-C are unclear and beyond the scope of the current manuscript. A more detailed exposition on exploiting Floquet prethermal states for quantum sensing will be presented elsewhere.

Approach to prethermal plateau – Finally, let us elucidate how the nuclear spins approach the Floquet prethermal plateau [56], focusing attention on regime **I** of Fig. 3A. We observe transients in the survival probability leading into the plateau; this is shown for two choices of the flip-angle ϑ in Fig. 5A ($\vartheta\approx\pi/2$ and $\vartheta\approx\pi/4$) respectively. High SNR allows us to track the oscillatory dynamics after every pulse, providing a window into how the approximately time-independent Hamiltonian is established. Moreover, the prethermal plateau level is itself dependent on ϑ.

The transients last for $t\approx10$ms, which is approximately the total lifetime for the original FID, and is of the order of magnitude of $\|\mathcal{H}_{dd}\|^{-1}$ (see Fig. 3A). As Fig. 5B indicates, the oscillation periodicity is closely related to the flip angle employed; for $\vartheta\approx\pi/2$, for instance, the oscillations occur at a fourth of the frequency of the Floquet drive ω. To see this more clearly, Fig. 5C shows the respective Fourier transforms in a 10ms region. Plotted against ω, we identify harmonics of the oscillatory dynamics (numbers). For $\vartheta\approx\pi/4$ (lower panels in Fig. 5B-C), we recognize a primary harmonic and higher harmonics at $\approx n\omega/8$, where n is an integer.

Intuitively, this characteristic periodicity can be thought of as arising from the number of pulses N_k required to return the Floquet unitary to a prior configuration; *i.e.* such that the toggling frame Hamiltonian after $2N_k$ pulses is equivalent to that after N_k, $\mathcal{H}^{(2N_k)}=\mathcal{H}^{(N_k)}$. This corresponds to effectively completing a 2π rotation of the Hamiltonian in the toggling frame. Four pulses are therefore needed for $\vartheta=\pi/2$ in Fig. 5A. In general, the primary harmonic frequency is expected to be at frequency $f=\vartheta/(2\pi\tau)$. Experiments confirm this picture; we extract the oscillation frequencies in regime **I** as a function of ϑ, and they fall neatly onto three straight lines for the three harmonics (see Fig. 5D). We hypothesize that the higher harmonics arise from bilinear and trilinear terms in the density matrix produced by dipolar evolution. The experimentally measured slopes are in the ratio 1:1.98:2.93, close to the 1:2:3 pattern expected. The precise deviation of these ratios from 1:2:3, as well as the nonzero intercept of the extrapolated fits in Fig. 5D are experimental surprises that will be the subject of future work. We note that this question is outside the scope of a Magnus expansion treatment, and relates to how an average Hamiltonian is established in the first place.

In conclusion, we have observed Floquet prethermalization of dipolar-coupled nuclear spins in a bulk solid at room temperature. The observed >90s-long prethermal lifetimes in diamond ^{13}C nuclei are over four orders of magnitude longer than free induction decay times, and significantly longer than in other systems. Our measurements unveil regimes of thermalization with a degree of clarity not accessible in previous NMR studies. Apart from fundamental insights, our work points to attractive opportunities possible via Floquet control in hyperpolarizable, dilute and low-γ_n nuclear networks. Protection and continuous interrogation of spins along a Bloch transverse axis for ~10min periods opens avenues for high-sensitivity magnetometers, gyroscopes [57, 58], and spin sensors [59] constructed out of hyperpolarized prethermal ^{13}C nuclei.

[1] L. F. Santos, The quick drive to pseudo-equilibrium, Nature Physics , 1 (2021).

[2] L. DâĂŹAlessio and M. Rigol, Long-time behavior of isolated periodically driven interacting lattice systems, Physical Review X **4**, 041048 (2014).

[3] N. Goldman and J. Dalibard, Periodically driven quantum systems: effective hamiltonians and engineered gauge fields, Physical review X **4**, 031027 (2014).

[4] M. Bukov, L. D'Alessio, and A. Polkovnikov, Universal high-frequency behavior of periodically driven systems: from dynamical stabilization to floquet engineering, Advances in Physics **64**, 139 (2015).

[5] D. A. Abanin, W. De Roeck, and F. Huveneers, Exponentially slow heating in periodically driven many-body systems, Physical review letters **115**, 256803 (2015).

[6] A. Lazarides, A. Das, and R. Moessner, Equilibrium states of generic quantum systems subject to periodic driving, Physical Review E **90**, 012110 (2014).

[7] T. Kuwahara, T. Mori, and K. Saito, FloquetâĂŞmagnus theory and generic transient dynamics in periodically driven many-body

quantum systems, Annals of Physics **367**, 96 (2016).

[8] M. Bukov, S. Gopalakrishnan, M. Knap, and E. Demler, Prethermal floquet steady states and instabilities in the periodically driven, weakly interacting bose-hubbard model, Physical review letters **115**, 205301 (2015).

[9] D. A. Abanin, W. De Roeck, W. W. Ho, and F. Huveneers, Effective hamiltonians, prethermalization, and slow energy absorption in periodically driven many-body systems, Physical Review B **95**, 014112 (2017).

[10] S. A. Weidinger and M. Knap, Floquet prethermalization and regimes of heating in a periodically driven, interacting quantum system, Scientific reports **7**, 1 (2017).

[11] D. J. Luitz, R. Moessner, S. Sondhi, and V. Khemani, Prethermalization without temperature, Physical Review X **10**, 021046 (2020).

[12] K. Singh, C. J. Fujiwara, Z. A. Geiger, E. Q. Simmons, M. Lipatov, A. Cao, P. Dotti, S. V. Rajagopal, R. Senaratne, T. Shimasaki, M. Heyl, A. Eckardt, and D. M. Weld, Quantifying and controlling prethermal nonergodicity in interacting floquet matter, Phys. Rev. X **9**, 041021 (2019).

[13] D. V. Else and C. Nayak, Classification of topological phases in periodically driven interacting systems, Physical Review B **93**, 201103 (2016).

[14] V. Khemani, A. Lazarides, R. Moessner, and S. L. Sondhi, Phase structure of driven quantum systems, Physical review letters **116**, 250401 (2016).

[15] H. Zhao, F. Mintert, R. Moessner, and J. Knolle, Random multipolar driving: Tunably slow heating through spectral engineering, Phys. Rev. Lett. **126**, 040601 (2021).

[16] O. Howell, P. Weinberg, D. Sels, A. Polkovnikov, and M. Bukov, Asymptotic prethermalization in periodically driven classical spin chains, Physical review letters **122**, 010602 (2019).

[17] A. Rubio-Abadal, M. Ippoliti, S. Hollerith, D. Wei, J. Rui, S. Sondhi, V. Khemani, C. Gross, and I. Bloch, Floquet prethermalization in a bose-hubbard system, Physical Review X **10**, 021044 (2020).

[18] K. Viebahn, J. Minguzzi, K. Sandholzer, A.-S. Walter, M. Sajnani, F. Görg, and T. Esslinger, Suppressing dissipation in a floquet-hubbard system, Physical Review X **11**, 011057 (2021).

[19] M. Ueda, Quantum equilibration, thermalization and prethermalization in ultracold atoms, Nature Reviews Physics , 1 (2020).

[20] P. Peng, C. Yin, X. Huang, C. Ramanathan, and P. Cappellaro, Floquet prethermalization in dipolar spin chains, Nature Physics , 1 (2021).

[21] C. Yin, P. Peng, X. Huang, C. Ramanathan, P. Cappellaro, et al., Prethermal quasiconserved observables in floquet quantum systems, Physical Review B **103**, 054305 (2021).

[22] J. Rovny, R. L. Blum, and S. E. Barrett, Observation of discrete-time-crystal signatures in an ordered dipolar many-body system, Physical review letters **120**, 180603 (2018).

[23] M. M. Maricq, Spin thermodynamics of periodically time-dependent systems: The quasistationary state and its decay, Physical Review B **36**, 516 (1987).

[24] M. M. Maricq, Long-time limitations of the average hamiltonian theory: A dressed-states viewpoint, in *Advances in Magnetic Resonance: The Waugh Symposium* (Academic Press, 1990) pp. 151–182.

[25] D. Sakellariou, P. Hodgkinson, and L. Emsley, Quasi equilibria in solid-state nmr, Chem. Phys. Lett. **293**, 110 (1998).

[26] D. Sakellariou, P. Hodgkinson, S. Hediger, and L. Emsley, Experimental observation of periodic quasi-equilibria in solid-state nmr, Chem. Phys. Lett. **308**, 381 (1999).

[27] J. b. Waugh, Equilibrium and ergodicity in small spin systems, Molecular Physics **95**, 731 (1998).

[28] R. Bruschweiler and R. Ernst, Non-ergodic quasi-equilibria in short linear spin 12 chains, Chem. Phys. Lett. **264**, 393 (1997).

[29] T. D. Ladd, D. Maryenko, Y. Yamamoto, E. Abe, and K. M. Itoh, Coherence time of decoupled nuclear spins in silicon, Phys. Rev. B **71**, 014401 (2005).

[30] Y. Dong, R. Ramos, D. Li, and S. Barrett, Controlling coherence using the internal structure of hard π pulses, Phys. Rev. Lett. **100**, 247601 (2008).

[31] C. L. Degen, F. Reinhard, and P. Cappellaro, Quantum sensing, Reviews of modern physics **89**, 035002 (2017).

[32] C. Fleckenstein and M. Bukov, Thermalization and prethermalization in periodically kicked quantum spin chains, Phys. Rev. B **103**, 144307 (2021).

[33] E. Reynhardt and C. Terblanche, 13c relaxation in natural diamond, Chemical physics letters **269**, 464 (1997).

[34] A. Ajoy, B. Safvati, R. Nazaryan, J. Oon, B. Han, P. Raghavan, R. Nirodi, A. Aguilar, K. Liu, X. Cai, et al., Hyperpolarized relaxometry based nuclear t 1 noise spectroscopy in diamond, Nature communications **10**, 1 (2019).

[35] D. Hoult, The nmr receiver: a description and analysis of design, Progress in Nuclear Magnetic Resonance Spectroscopy **12**, 41 (1978).

[36] A. Ajoy, K. Liu, R. Nazaryan, X. Lv, P. R. Zangara, B. Safvati, G. Wang, D. Arnold, G. Li, A. Lin, et al., Orientation-independent room temperature optical 13c hyperpolarization in powdered diamond, Sci. Adv. **4**, eaar5492 (2018).

[37] A. Ajoy, R. Nazaryan, K. Liu, X. Lv, B. Safvati, G. Wang, E. Druga, J. Reimer, D. Suter, C. Ramanathan, et al., Enhanced dynamic nuclear polarization via swept microwave frequency combs, Proceedings of the National Academy of Sciences **115**, 10576 (2018).

[38] See supplementary online material.

[39] Video showing full dataset of Fig. 4: `https://www.youtube.com/watch?v=uLKIR_XM_FQ` (2021).

[40] E. Ostroff and J. Waugh, Multiple spin echoes and spin locking in solids, Physical Review Letters **16**, 1097 (1966).

[41] W.-K. Rhim, D. Burum, and D. Elleman, Multiple-pulse spin locking in dipolar solids, Physical Review Letters **37**, 1764 (1976).

[42] W.-K. Rhim, D. Burum, and D. Elleman, Calculation of spin–lattice relaxation during pulsed spin locking in solids, The Journal of Chemical Physics **68**, 692 (1978).

[43] U. Haeberlen, *High Resolution NMR in Solids: Selective Averaging* (Academic Press Inc., New York, 1976).

[44] W. Magnus, On the exponential solution of differential equations for a linear operator, Communications on Pure and Applied Mathematics **7**, 649 (1954).

[45] R. M. Wilcox, Exponential operators and parameter differentiation in quantum physics, Journal of Mathematical Physics **8**, 962 (1967).

[46] S. Blanes, F. Casas, J. Oteo, and J. Ros, The magnus expansion and some of its applications, Physics Reports **470**, 151 (2009).

[47] A. Ajoy, R. Nirodi, A. Sarkar, P. Reshetikhin, E. Druga, A. Akkiraju, M. McAllister, G. Maineri, S. Le, A. Lin, et al., Dynamical decoupling in interacting systems: applications to signal-enhanced hyperpolarized readout, arXiv preprint arXiv:2008.08323 (2020).

[48] H. Y. Carr and E. M. Purcell, Effects of diffusion on free precession in nuclear magnetic resonance experiments, Phys. Rev. **94**, 630 (1954).

[49] R. Ernst, G. Bodenhausen, and A. Wokaun, *Principles of nuclear magnetic resonance in one and two dimensions* (Clarendon Press Oxford, 1987).

[50] I. Lowe, Free induction decays of rotating solids, Physical Review Letters **2**, 285 (1959).

[51] M. Pfender, P. Wang, H. Sumiya, S. Onoda, W. Yang, D. B. R. Dasari, P. Neumann, X.-Y. Pan, J. Isoya, R.-B. Liu, et al., High-resolution spectroscopy of single nuclear spins via sequential weak measurements, Nature communications **10**, 1 (2019).

[52] Video showing full dataset of Fig. 5: https://www.youtube.com/watch?v=8NI7Zzugi4o (2021).

[53] D. Tse and S. Hartmann, Nuclear spin-lattice relaxation via paramagnetic centers without spin diffusion, Physical Review Letters **21**, 511 (1968).

[54] N.-a. Lin and S. Hartmann, Nuclear spin-lattice relaxation in ca f 2 via paramagnetic centers for short correlation time when spin diffusion is inhibited, Physical Review B **8**, 4079 (1973).

[55] C. Fleckenstein and M. Bukov, Prethermalization and thermalization in periodically driven many-body systems away from the high-frequency limit, Phys. Rev. B **103**, L140302 (2021).

[56] A. Haldar, R. Moessner, and A. Das, Onset of floquet thermalization, Physical Review B **97**, 245122 (2018).

[57] A. Ajoy and P. Cappellaro, Stable three-axis nuclear-spin gyroscope in diamond, Phys. Rev. A **86**, 062104 (2012).

[58] M. Ledbetter, K. Jensen, R. Fischer, A. Jarmola, and D. Budker, Gyroscopes based on nitrogen-vacancy centers in diamond, Physical Review A **86**, 052116 (2012).

[59] M. Abobeih, J. Randall, C. Bradley, H. Bartling, M. Bakker, M. Degen, M. Markham, D. Twitchen, and T. Taminiau, Atomic-scale imaging of a 27-nuclear-spin cluster using a quantum sensor, Nature **576**, 411 (2019).